Probing the existing magnetic phases in $Pr_{0.5}Ca_{0.5}MnO_3$ (PCMO) nanowires and nanoparticles: magnetization and magneto-transport investigations

2010 J. Phys.: Condens. Matter 22 116004

(http://iopscience.iop.org/0953-8984/22/11/116004)

J. Phys.: Condens. Matter **22** (2010) 116004 (9pp) doi:10.1088/0953-8984/22/11/116004

Probing the existing magnetic phases in $Pr_{0.5}Ca_{0.5}MnO_3$ (PCMO) nanowires and nanoparticles: magnetization and magneto-transport investigations

S S Rao[1,2] and S V Bhat[1]

[1] Department of Physics, Indian Institute of Science, Bangalore-560012, India
[2] INPAC—Institute for Nanoscale Physics and Chemistry, Semiconductor Physics Laboratory, K.U.Leuven, Celestijnenlaan 200 D, B-3001 Leuven, Belgium

E-mail: ssrao@physics.iisc.ernet.in, Srinivasarao.singamaneni@fys.kuleuven.be and svbhat@physics.iisc.ernet.in

Received 19 September 2009, in final form 28 December 2009
Published 23 February 2010
Online at stacks.iop.org/JPhysCM/22/116004

Abstract
We show from conventional magnetization measurements that the charge order (CO) is completely suppressed in 10 nm $Pr_{0.5}Ca_{0.5}MnO_3$ (PCMO 10) nanoparticles. Novel magnetization measurements, designed by a special high field measurement protocol, show that the dominant ground state magnetic phase is ferromagnetic-metallic (FM-M), which is an equilibrium phase, which coexists with the residual charge ordered anti-ferromagnetic phase (CO AFM) (an arrested phase) and exhibits the characteristic features of a 'magnetic glassy state' at low temperatures. It is observed that there is a drastic reduction in the field required to induce the AFM to FM transition (∼5–6 T) compared to their bulk counterpart (∼27 T); this phase transition is of first order in nature, broad, irreversible and the coexisting phases are tunable with the cooling field. Temperature-dependent magneto-transport data indicate the occurrence of a size-induced insulator–metal transition (T_{M-I}) and anomalous resistive hysteresis (R–H) loops, pointing out the presence of a mixture of the FM-M phase and AFM-I phase.

(Some figures in this article are in colour only in the electronic version)

1. Introduction

The occurrence of charge order (CO) in doped perovskite manganites of type $RE_{1-x}A_xMnO_3$ (RE = trivalent rare earth ion, A = divalent alkaline earth ion) is currently a much-studied phenomenon. The CO state, characterized by a long-range ordering of the Mn^{3+} and Mn^{4+} ions, is the result of a complicated competition between Coulomb interactions (between the charges), exchange interactions (between the Mn moments) and the electron–lattice coupling through Jahn–Teller (JT) distortions of the oxygen octahedron surrounding the Mn^{3+} ion. For example, in $Pr_{0.5}Ca_{0.5}MnO_3$ (PCMO), which is a narrow band CO anti-ferromagnetic insulating manganite (AFM-I), a favourable situation for CO is at $x = 0.5$, with equal amounts of Mn^{3+} and Mn^{4+} ions. The ordering is of the CE (charge exchange)-type checkerboard pattern, accompanied by dz^2-type orbital ordering of the e_g orbitals on the Mn^{3+} sites in a zigzag arrangement, and, at lower temperatures, by AFM ordering of the Mn moments. The stability of the CO phase is controlled by the e_g electron bandwidth of the material, and is less stable away from the $x = 0.5$ composition. The CO state is sensitive to the external perturbations like the magnetic field, electric field, impurity ion doping and irradiation with high energy rays [1–4]. When subjected to these perturbations it turns into a charged liquid metallic phase with FM order as the energy gap between the CO and FM phases decreases. For the same composition, in the nanoscale thin films of PCMO, the introduction of defects was shown to melt the CO phase and consequently the CO was shown to be softened [5]. Down-sizing the physical

limits of these materials—grown in various morphological shapes and sizes by employing diverse methods—is shown to exhibit novel properties [6–8]. The effect of size reduction down to the nanoscale has been manifested in the observation of novel properties. To illustrate this, the single-crystalline nanoribbons of Sr_3MnO_6 are shown to exhibit FM whereas its bulk counterpart is AFM [9]. On the other hand, for example, very recently [10] it has been shown that ferromagnetism is collapsed when nanowires of Ni, Co and Fe break into atomic dimensions. To draw further attention towards the inorganic nanoscale entities, remarkably, by taking the advantage of state-of-the-art nanofabrication techniques, the magnetization and magneto-transport properties of single nanowires and hollow cylindrical-single nanotubes of CMR manganite have been measured [11, 12]. Recently, much attention has been paid to the properties of CO AFM manganites (of various melting points) at the nanoscale [13–21], and it is convincingly accepted and reported that the solution-grown nanoscale CO AFM manganites exhibit weakening/suppression of the CO phase and a size-induced FM phase in place of the AFM phase—as identified by conventional magnetization, transport and electron magnetic resonance (EMR) measurements. All the documented observations point to the fact that the CO phase is softened even though the root cause for such a change is still under intense debate. From the unsaturated M–H loops and from the observed lower classical saturation magnetization (than expected for a fully aligned spin moment), it may be inferred that size reduction could not suppress the CO phase completely, and the presence of a residual CO phase inhibits the complete transformation of the AFM-I phase to the FM-M phase.

In our earlier publication [13], we have reported preliminary results on PCMO nanowires (PCMO NWs), where it was shown that the CO phase is weakened and there is a switchover from the AFM phase to the FM phase as obtained from conventional static DC magnetization and dynamic X-band (frequency = 9.43 GHz) electron spin resonance (ESR) measurements. In another report [14], in the case of $Nd_{0.5}Ca_{0.5}MnO_3$ (NCMO) nanoparticles, it was shown that the CO phase is suppressed and the CO fraction increases with the particle size. There is a switchover from AFM phase to FM phase, and a size-induced insulator–metal transition (T_{M-I}) and CMR of 99.7% are observed. In our recent publication [15], in the case of $Pr_{0.5}Sr_{0.5}MnO_3$ (PSMO) NWs and nanoparticles, we have shown that the CO phase is collapsed and there is a size-induced FM phase which appears, coexisting with the residual AFM phase. With regard to the size-induced T_{M-I}, the nanoscale particles show complex temperature-dependent magnetoanisotropic behaviour in contrast with that of the bulk counterpart. Size-induced CO phase collapse was shown to be not common for all the CO manganites, as is observed in the case of $Bi_{0.5}Ca_{0.5}MnO_3$ (BCMO) and $Bi_{0.5}Sr_{0.5}MnO_3$ (BSMO) nanoparticles. They are shown to retain their bulk properties (up to room temperature), in confirmation of their robust CO phase and apparently a magnetic field of more than 50 T is needed to melt the CO phase [16]. Very recently [17], we have shown that, in the case of NCMO nanoparticles, by following a novel magnetization protocol, magneto-transport and EMR measurements, the residual CO fluctuations are still present even in 10 nm NCMO particles.

Nevertheless, weakly [15] and moderately [13, 14] robust CO manganites are shown to exhibit an FM phase with the weakening/suppression of the CO phase, if not for highly robust CO manganites [16]. Later, several experimental and theoretical reports [18–21] have appeared in the literature in support of our results [13–17], though the origin of such an observation is still being investigated. However, the questions yet to be addressed are: what is the predominant ground (equilibrium) state? What are the coexisting magnetic phases? What is the nature of the magnetic phase transition? And what is the magneto-resistive behaviour of these nanoscale entities? Here, in this paper, we aim to address the above issues by conducting detailed temperature-and magnetic-field-dependent magnetization and transport measurements on PCMO nanoparticles (PCMO 10, PCMO 20 and PCMO 40) and PCMO nanowires (PCMO NWs). In this paper, we show that, using moderate magnetic fields (∼5–6 T), the AF-I (residual) phase can be converted into the FM-M phase at low temperatures. However, we find that the system does not get back to its original magnetic state (AFM-I) when the field is reduced isothermally, showing an irreversible first-order phase transition. We present the results to show that nanoscale PCMO (PCMO 20 and PCMO 40) exhibit the features of a magnetic glassy state. with the FM-M as the equilibrium phase and AFM-I as the arrested phase, similar to the 2.5% Al-doped PCMO and in contrast to $La_{0.5}Ca_{0.5}MnO_3$ (LCMO) [22–24]. We believe that these results may have important implications for magnetic switching devices and in magnetic memory applications.

In the phase diagram, the composition of interest is at $x = 0.5$. It is noted that at this composition this material undergoes a transition from a paramagnetic charge disordered phase to a charge ordered phase at temperature $T_{CO} = 245$ K and from the CO phase to an AFM phase at temperature $T_N = 175$ K as the material is cooled down from room temperature [25]. This material exhibits insulating behaviour all through the temperature range (4–300 K) with a sharp rise in resistivity at T_{CO}. PCMO crystallizes in orthorhombic phase with the space group $Pbnm$. Lattice parameters are $a = 5.404\,28$ Å, $b = 7.612\,7531$ Å, $c = 5.394\,14$ Å and the unit cell volume $V = 221.92$ Å^3 [26]. In section 2, we give the results obtained from various characterization techniques. In section 3, we present and discuss the results related to our conventional and specially designed high magnetic field magnetization measurements. The results obtained from magneto-transport measurements on various samples are presented and discussed in section 4, followed by the conclusions in section 5.

2. Nanoparticles: preparation and characterization

Nanoparticles of PCMO were prepared by the polymeric precursor sol–gel method, also known as the Pechini method [14–17]. Though in the original method dissolution of the precursors of cations in an aqueous citric acid solution was used and ethylene glycol was used as a promoter of citrate

Table 1. Variation of lattice parameters and unit cell volume of the nanosamples in comparison with that of the bulk.

Sample name	Crystallite size (nm) (from XRD)	Particle size (nm) (from TEM)	a (Å)	b (Å)	c (Å)	V (Å)^3
PCMO 10	8 ± 3	10	5.473 4	7.563 4	5.4123	224.0557
PCMO 20	15 ± 3	20	5.462 7	7.589 8	5.4096	224.2863
PCMO 40	35 ± 2	40	5.455 6	7.598 7	5.4049	223.7019
PCMO NW	43 ± 2	$\sim$50	5.446 4	7.603 1	5.3962	223.0842
PCMO BULK	μm	μm	5.404 28	7.612 7531	5.3941	221.92

polymerization, it has been shown to work in the absence of citric acid as well [27] and we have used the latter procedure. In this technique, the polymerized ethylene glycol assists in forming a close network of cations from the precursor solution and helps the reaction enabling the phase formation at low temperatures. The gel forms a resin and the high viscosity of the resin prevents different cations from segregating and ensures a high level of homogeneity. In our preparation, nitrates of praseodymium, calcium and manganese were used as precursors and were dissolved in their stoichiometric ratio in triple-distilled water. An equal amount of ethylene glycol was added with continuous stirring. The solution was heated and the water evaporated on a hot plate whose temperature was increased gradually to 180 °C till a thick sol was formed. The sol in turn was heated in a furnace at 250 °C for about 6 h till a porous material is obtained as a result of the complete removal of water molecules. This was further calcined at 600 °C and crystalline nanoparticles of PCMO of average size $\sim$10 nm were obtained [17]. We designate this sample as PCMO 10. Parts of this sample were further heated at 700 and 900 °C for another 6 h to obtain samples with increased averaged grain size (20 and 40 nm). These samples are labelled as PCMO 20 and PCMO 40 [17]. PCMO nanowires (PCMO NWs) were fabricated by the hydro-thermal method and were characterized by several techniques [13]. For comparison purposes, a PCMO bulk sample was also prepared, using the method of solid state reaction and will be labelled as PCMO BULK [13]. The crystalline sizes of the three nanoparticles calculated from the full width at half-maximum of the diffraction peaks according to the Scherrer formula, are about 8, 15 and 35 nm for PCMO 10, PCMO 20 and PCMO 40, respectively. From the TEM images, the average particle sizes of the above samples are 10, 20 and 40 nm, respectively. As can be inferred from these numbers, the value from the TEM images is larger than that from the XRD pattern, which may imply that the nanoparticles are aggregated. The lattice parameters (extracted from Rietveld refinement analysis of the XRD pattern) and lattice volumes of the nanosamples in comparison with the bulk are shown in table 1. In light of the data presented in this table, it may be inferred that the lattice parameters do not vary appreciably with the reduction of particle size.

3. Magnetization measurements

Detailed magnetization measurements have been performed on the tightly packed materials of PCMO 10, PCMO 20, PCMO 40 and PCMO NWs. Three different commercial magnetometers were used for this task: (1) a Quantum Design SQUID magnetometer driven in the temperature range from 10 to 300 K, and with the magnetic field range from -5 to $+5$ T; (2) a Quantum Design PPMS VSM having the facility to vary the temperature from 2 to 300 K and the range of the magnetic field from -14 to $+14$ T and (3) a Quantum Design PPMS VSM having the temperature sweep facility from 2 K to 300 K and the magnetic field ranging from -9 to $+9$ T. The conditions employed for each measurement are described in the figure captions of each graph.

Figure 1(a) shows the variation in magnetization with temperature of PCMO 10 measured at 0.1 T after cooling the sample down to 2 K in zero field (ZFC) and the data was taken while warming up. A peak at around 50 K may indicate the 'blocking temperature (T_b)' [15]. The magnetization of PCMO 10 at 1 T is also measured during field-cooled cooling (FCC) and field-cooled warming (FCW). The observed broad non-hysteretic and sharp rise at the lower temperatures indicate the onset of a ferromagnetic transition. In this figure, no indication of the CO peak at 245 K is observed, indicating that the CO phase is completely suppressed, the saturated magnetic moment is not achieved fully even at 2 K, and it does not seem to follow Bloch's 3/2 law—used to describe the temperature-dependent magnetization behaviour of classical homogeneous ferromagnets. In figure 1(b), the variation of magnetization of PCMO 20 and PCMO 40 with the temperature measured under FCC conditions and at 1 T is shown. In addition to the sharp rise in magnetization (M) at around 150 K, a broad hump at around 250 K is also seen in PCMO 20, and this hump increases with the increase in particle size from 20 to 40 nm—showing the increase of CO fraction with particle size. Figure 1(c) depicts the M–H curves of PCMO 10 at temperatures 2, 20, 40, 60, 80, 100 and 120 K, as obtained by sweeping the magnetic field from 0 $\rightarrow$ 2 T $\rightarrow$ 0 $\rightarrow$ -2 T $\rightarrow$ 0 $\rightarrow$ 2 T. It is clearly observed that, at 2 K, PCMO 10 exhibits a ferromagnetic hysteresis behaviour with unsaturated magnetization, and this ferromagnetic nonlinear magnetization behaviour with the magnetic field gradually changes to paramagnetic (linear) behaviour as the temperature grows from 2 to 120 K. Similar experiments have been performed on PCMO NWs at various temperatures and the results are presented in figure 1(d). A clear opening of the M–H loop is observed at 2 K and it slowly closes, turning into a linear M–H curve upon heating. In order to compare the magnetic hysteretic behaviour of these nanosamples, M–H measurements were carried out on the PCMO BULK at 10 K and the obtained perfect linear M–H curve is shown in figure 1(e), indicating the AFM nature of PCMO BULK at low temperatures. Size-induced FM ESR signals are observed

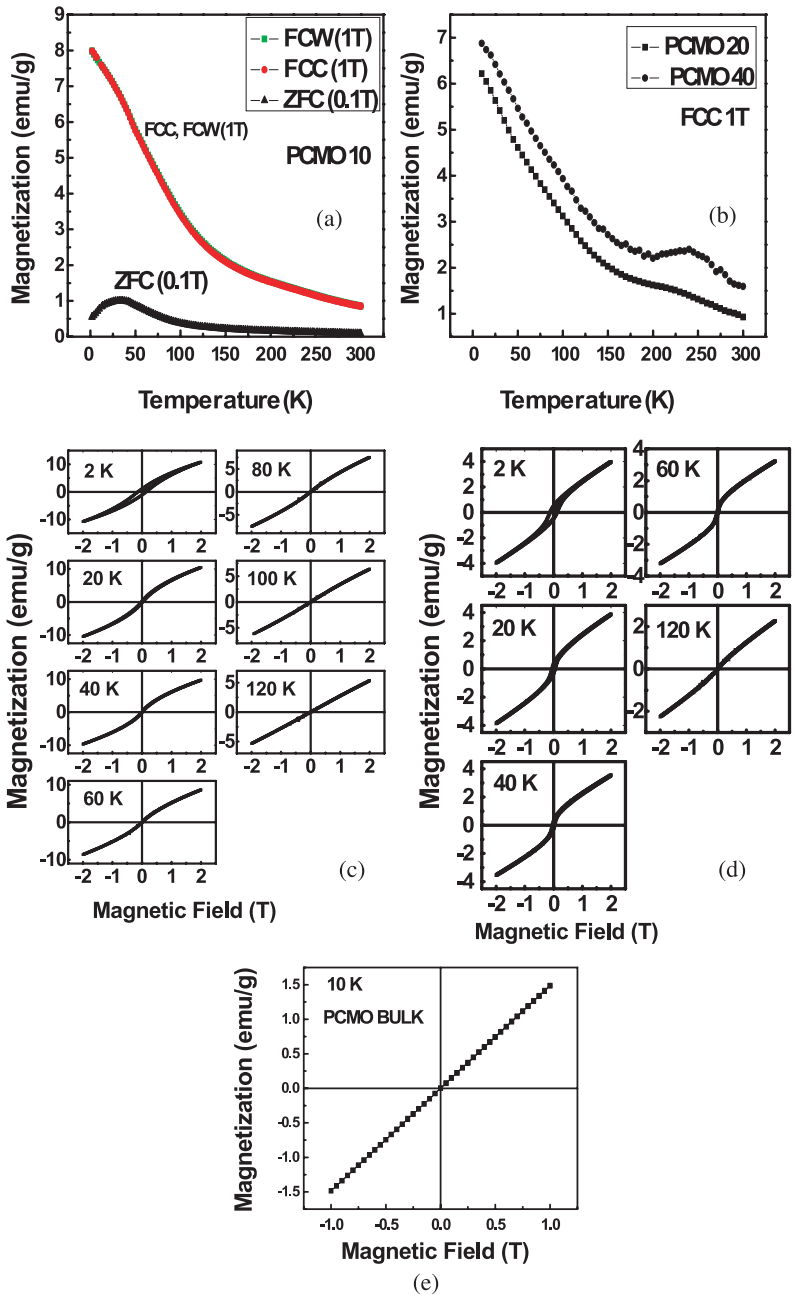

Figure 1. Variation of magnetization with temperature of PCMO 10 (a), and PCMO 20 and PCMO 40 (b), respectively, at different conditions as indicated in the figure. Isothermal M–H loops of PCMO 10 measured at different temperatures of 2, 20, 40, 60, 80, 100 and 120 K (c). Isothermal M–H loops of PCMO NWs measured at different temperatures of 2, 20, 40, 60 and 120 K (d). M–H behaviour of PCMO BULK at 10 K (e).

from PCMO NW, PCMO 10, PCMO 20 and PCMO 40 and are shown to be absent in PCMO BULK at lower temperatures as it shows AFM behaviour [17].

With the motivation to understand the size-induced ground state magnetic phase of PCMO NWs and PCMO nanoparticles (PCMO 10, PCMO 20 and PCMO 40), isothermal magnetization experiments were performed at 5 K (after cooling the samples from room temperature down to 5 K) on all the samples (PCMO 10, PCMO 20, PCMO 40 and PCMO NWs) by sweeping the magnetic field from 0 → 14 T → 0 → 14 T (the limit of the magnetic field), and the obtained results are shown in figure 2. Several features in this figure merit attention. The results obtained on the PCMO 10, PCMO 20 and PCMO 40 samples mimic the ones reported earlier in the case of bulk polycrystalline 2.5% Al-doped PCMO [22–24]. Hence, we use similar arguments here to explain our results. In the case of PCMO 10, as shown in figure 2(a), the initial field increasing cycle (I) shows a quasi-linear increase in the magnetization at lower fields (up to about 8–9 T), then it undergoes a broad field-induced transition to FM (from the small residual AFM phase) and does not attain its spin-aligned moment value (3.5 μ_B/f.u.) even at 14 T.

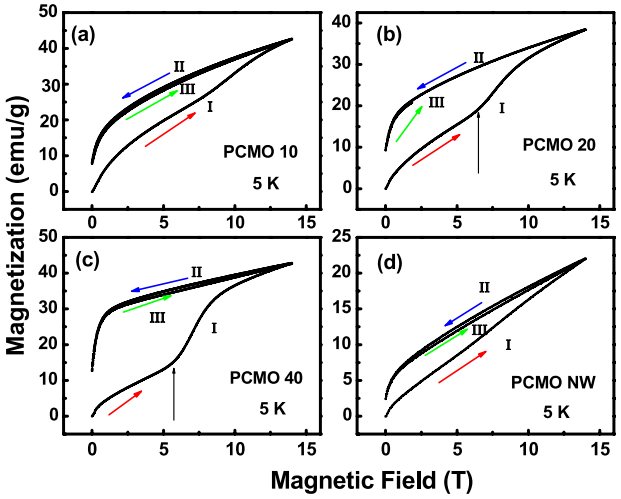

Figure 2. Isothermal M–H results obtained at 5 K on PCMO 10 (a), PCMO 20 (b), PCMO 40 (c) and PCMO NW (d) with the magnetic field cycling between forward and reverse directions as shown by the pointed arrow. Red arrows (I) virgin curve, blue (II) and green (III) arrows the envelope curves, black vertical arrows show the field-induced first-order phase transition (FOPT).

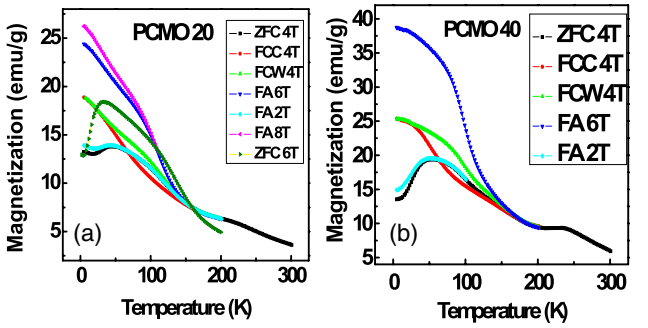

Figure 3. After cooling PCMO 20 in 2, 6 and 8 T, the field is isothermally changed to 4 T at 5 K and the magnetization is measured while warming (FA 2 T, FA 6 T, FA 8 T). The variation of magnetization with the temperature in zero-field cooling (4 and 6 T), field-cooled cooling and warming at 4 T is shown as ZFC 4 T, ZFC 6 T and FCCW 4 T (a). A similar protocol was followed as mentioned above in the case of PCMO 40 to measure the magnetization with temperature (b).

However, the field decreasing cycle (II) and the next field increasing cycles (III) do not show the reverse transition to the initial AFM (residual) state—pointing out an anomaly in the field-induced first-order transition. On decreasing the field to zero, the magnetization approaches zero with a soft FM-like behaviour with unsaturated magnetic moments (at 14 T, 5 K). In the case of PCMO NWs (from figure 2(d), virgin branch I), the magnetization increases linearly with the field up to 14 T, exhibiting no indications of a field-induced first-order transition (unlike PCMO 10, PCMO 20 and PCMO 40), and the rest of the field cycling (II and III) results resemble those of PCMO 10, PCMO 20 and PCMO 40. From these field cycling experiments on PCMO NWs, it can be inferred that the larger fraction of AFM phase may be present, and hence, apparently, still higher magnetic fields need to be employed in order to induce phase transition.

Now, we focus our attention on the isothermal high field M–H branches of PCMO 20 and PCMO 40 (figures 2(b) and (c)). The initial field increasing cycle (I) of PCMO 20 and PCMO 40 shows a linear increase in magnetization. Interestingly, it is observed that at around 6.5 T (in the case of PCMO 20) and at 6 T (in the case of PCMO 40), there is a sudden rise in the magnetization. It could be either due to the melting of the residual CO phase present in the PCMO 20 and PCMO 40 samples by the application of a magnetic field or it could be due to the field-induced first-order phase transition (FOPT) from the AFM phase (residual) to the FM phase. Figures 2(b) and (c) show that the ZFC AF state transforms into an FM state with an increase in the field above 6 T, but the initial AF state does not recover even after the field is reduced (II) from 14 T to zero, though a small hysteresis is observed in the subsequent consecutive H cyclings (III). The subsequent H-increasing (III) curve shows no signature of the AF to FM transition, indicating that the remanent state is FM to a large extent, though the saturation magnetization for fully FM manganite material has not attained its expected value (3.5 μ_B/f.u.) at the highest magnetic fields (14 T) reached and at the temperature 5 K, also showing negligible coercivity, and also without any observable opening around zero magnetic field. From these figures, the common feature observed is that, with the decrease in magnetic field, the magnetization decreases to zero, resembling a soft FM-like phase. Another notable observation made here is that the virgin curve lies outside the subsequent M–H traces in all these nanosystems, showing the clear irreversibility in the transition. The possible reasons for the observation of the virgin curve being outside the envelope can be found elsewhere [17, 28–32].

As was shown in the isothermal high field M–H measurements at 5 K, the residual AF-I state (of PCMO 10, PCMO 20 and PCMO 40) can be converted into an FM-M state by applying moderate magnetic fields. However, we find that the system does not go back to its original AF-I state when the field is withdrawn isothermally. Then the question arises regarding the equilibrium phase: is it an FM-M phase or an AF-I phase? In order to remove the ambiguity about the low temperature equilibrium phase, we follow a specially designed uncommon measurement protocol, namely 'cooling and heating in unequal fields (CHUE)' [24]. Figure 3(a) presents the variation of magnetization with the temperature when PCMO 20 is subjected to different conditions. Here, we describe the meanings of the terms used in the graph. ZFC 4 T and ZFC 6 T indicate that magnetization is measured during the heating run at 4 T and 6 T, respectively, after the system is cooled in zero field. FCCW 4 T is used when magnetization is measured at 4 T while the system is being cooled down/warmed up in the presence of a 4 T magnetic field. FA (field annealing) 2 T, 6 T and 8 T mean that the system is cooled down to 5 K in the presence of magnetic fields 2 T, 6 T and 8 T, respectively, and the magnetization is measured at 4 T while warming up. From this figure, the observed hysteresis between the FCC and FCW curves in M–T in a temperature range of about 25–150 K indicates a broad first-order phase transition (FOPT) from the AF-I to the FM-M

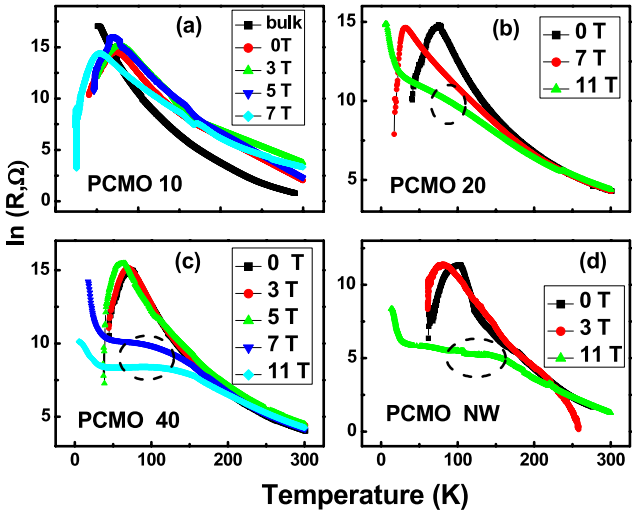

Figure 4. Variation of resistance ln R (R = resistance) with temperature of PCMO 10 (a), PCMO 20 (b), PCMO 40 (c) and PCMO NWs (d), respectively, at different magnetic fields including zero-field curves. In (a), the curve with the filled square symbol (■) shows the bulk in the absence of field.

state; the divergence of the ZFC curve below this temperature range in the same field shows the irreversibility in the transition and points towards nonergodicity at low temperature [22, 23]. The nonergodic behaviour at low temperature, which underlies the FOPT, becomes clear from the magnetic field annealing experimental results. From this figure, it is obvious that the cooling in lower fields results in lower magnetization in the same measuring field (4 T) because of the increasing amount of the trapped AF-I phase. It is interesting to note that, when the temperature is increased from 5 K the M–T behaviour for curves with cooling fields higher (6, 8 T) or lower (2 T) than the measuring field (4 T) are different. While the curves with cooling fields below 4 T remain almost the same till they approach the ZFC curve, the curves with cooling fields above 4 T remain distinct and finally merge with the FCW curve [22–24]. From this figure 3(a), related to PCMO 20, a sharp rise in the magnetization with the temperature (in the case of ZFC 4T, ZFC 6 T and FA 2 T) clearly indicates the rapid transformation of an untransformed AF-I phase fraction into the FM-M state. A similar observation is noticed even in PCMO 40 (ZFC 4 T, FA 2 T) M–T branches as shown in figure 3(b). Such a rapid transformation to the low temperature equilibrium phase when the temperature is applied to the system is similar to devitrification, evidence of a glassy state [24]. Similar arguments can be applied to PCMO 40 as well, whose results are shown in figure 3(b). From the established knowledge of doping-induced disorder manganite physics ([22–24] and references therein), though looking through the same perspective, the size reduction also plays a similar role (as that of disorder) in dictating the ground state magnetic and electronic phases. Current data may offer a solid testing ground to investigate the size-induced competing magnetic and electronic phases at various length scales.

The size-induced FM phase is fully corroborated by another independent, highly sensitive dynamical local probe, namely electron spin resonance (ESR), as shown in our earlier publication for PCMO nanowires [13]. From the conventional first harmonic X-band (9.43 GHz) ESR measurements performed on NCMO particles we confirm the size-induced FM down to the temperature 4 K [17]. Another noteworthy point is that ESR shows the presence of CO fluctuations even in 10 nm PCMO nanoparticles, as observed from the shallow minimum of the temperature dependence of EPR linewidth [17]. The same holds true for 10 nm NCMO particles as well [17].

The important conclusions drawn from the above section can be summarized below. The size reduction leads to the suppression and softening of the CO phase and induces an FM phase coexisting with an AFM phase, and the associated features point out the occurrence of FOPT. These coexisting magnetic phases are tunable by following the novel protocol in measuring the temperature-and magnetic-field-dependent magnetization. PCMO 20 and PCMO 40 are shown to exhibit the features of a magnetic glassy state.

4. Magneto-transport measurements—results and analysis

In order to examine the size-induced conductivity behaviour in the above-mentioned nanoscale systems, the temperature variation of static dc resistance measurements was carried out using an Oxford Instruments liquid helium bath cryostat in the temperature range 4–300 K. A linear four-probe method was used to measure the resistance. For the four-probe resistance measurements, pellets of 10 mm diameter were prepared under a pressure of 150 psi and then sintered at 300 °C for 2 h, ensuring that these parameters did not increase the particle size as we followed the similar procedure as earlier [14, 15, 17]. Silver–indium alloy was used to make the point contacts. The magneto-resistance (MR) measurements were carried out using a JANIS-made set-up with a maximum available field of 11 T. The temperature variation (10–300 K) resistance experiments were carried out at different fixed magnetic fields. At a fixed temperature, the magnetic-field-dependent resistance measurements were carried out by varying the field from −11 to +11 T.

Figures 4(a)–(d) show the variation of ln R (R = resistance) with temperature of PCMO 10, PCMO 20, PCMO 40 and PCMO NWs at different magnetic fields, respectively. The curve in figure 4(a) with the symbol (■) is that of PCMO BULK which shows an insulating behaviour throughout the temperature range studied, in conformity with the expected behaviour for insulating CO manganites. Surprisingly, as is clearly seen from these figures, all the nanosamples (PCMO 10, PCMO 20, PCMO 40 and PCMO NWs) show an insulator-to-metal-like transition at different temperatures (T_{M-I}) in the absence of magnetic field, i.e. size-induced metallicity. Similar size-induced metallic features were also observed in the case of NCMO, PSMO nanoparticles [14, 15, 17] and in PCMO nanoparticles of 15 nm [19]. The common feature observed in PCMO 20, PCMO 40 and PCMO NW is that, at 11 T, the T_{M-I} becomes broader and shifts to higher temperatures, as is shown in the encircled regions of figures 4(b)–(d). The resistance

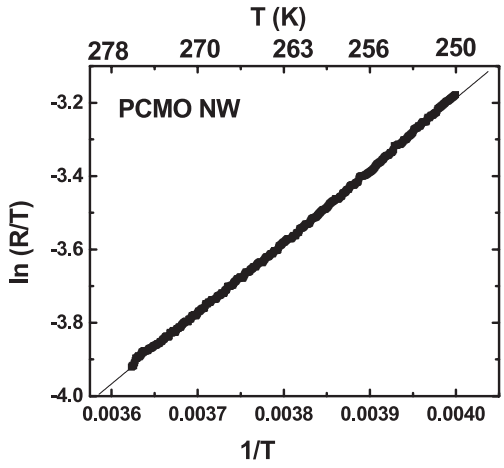

Figure 5. Adiabatic polaron activated fit [36] to the resistance behaviour in the paramagnetic region of PCMO NWs. The solid line is a fit to the experimental data points.

in some of the samples show an upturn at low temperatures, beginning at 30 K, and is predominantly seen at high magnetic fields. It is most likely that the magnetic fields modify the electronic properties of the grain boundary, which results in the upturn of the resistance. This observation could also be due to the grain boundary scattering and Coulomb blockade [33, 34]. Kumar *et al* [35] explained the low temperature upturn in the resistivity due to the electron–electron (e–e) interaction, Kondo effect and inelastic scattering in the case of thin films of micron-sized CMR manganites. They have observed the low temperature upturn in the resistivity even at 5 T. However, does this explanation hold true in nanoscale CO manganites? At this moment, we could not provide a quantitative analysis. The resistance in the FM-M phase is higher than that of the PM-I phase in all these nanomaterials both in the presence and in the absence of magnetic fields. This fact can be attributed to the grain boundary (GB) scattering in polycrystalline materials. In the paramagnetic insulating (PI) phase, the variation of resistance with temperature is well described by the activated adiabatic polaron hopping model [36] and the fits to the experimental curves are shown in figure 5 for PCMO NWs and is equally good for other samples as well (not shown). The energy of activation increases with the decrease of particle size from 150 meV (PCMO 40) to 153 meV (PCMO 20) though the increase is not significant. PCMO NWs show an activation energy of 167 meV. The activation energy decreases with applied magnetic field, as expected. We find that the current theoretical models fail to describe the transport properties of these nanoscale manganites in the size-induced FM phase (below 120 K), as was clearly shown elsewhere for similar systems [15].

Figures 6(a) and (b) show isothermal variation of resistance with magnetic field sweep (0–11 T) measured at different temperatures for PCMO 20 and PCMO 40, respectively, and figure 6(c) shows the variation of MR (at 11 T) with magnetic field for PCMO NWs. The pointed arrows are used to indicate the direction of the magnetic field sweep. At 11 T (PCMO 20, PCMO 40 and PCMO NWs) and at T_{M-I}, the calculated MR is found to be 99.7%, which is similar to the values observed in other prototype CMR oxides like $La_{0.67}Sr_{0.33}MnO_3$ and $La_{0.67}Ca_{0.33}MnO_3$. The high value of MR% observed in the FM-M phase of polycrystalline samples is attributed to the GB resistance. Negligible MR is observed in the PI phase of all the nanomaterials. For single-crystalline CMR manganites, the MR observed in the FM-M phase is very small since no GBs are present and all the spins are completely aligned. But if GBs are present (as in polycrystalline samples), they can act as scattering centres for the mobile electrons and will lead to the enhancement of resistivity and MR. At low temperatures the effect of GBs is dominant when the other mechanisms of scattering are negligible. Hence the observed high CMR (99.7%) at T_{M-I} indicates that the electron scattering at the domain GBs is the dominant mechanism of the electron transport at low temperatures. One noteworthy feature observed from these graphs is the anomalous variation of R/MR with magnetic field at the lowest temperatures observed in all the samples. This feature disappears with the increase of temperature (from 60 to 120 K). The second feature is the hysteretic resistance which is observed at all temperatures studied and the resistive hysteretic loop area decreases with the increase of temperature. The third observation is size-induced CMR (99.7% MR at 11 T) at T_{M-I} for all the samples. All these features could be the consequence of size-induced FM, metallicity and destabilized charge ordered (CO) phase.

From figures 6(a)–(c), at the lowest temperatures studied, it is noted that there is an upward rise in the resistance up to a certain value of the magnetic field (positive MR), and then the resistance drops down sharply (negative MR), and thereafter further variation of resistance with magnetic field is constant. The positive MR is observed in both forward and reverse field cycles and occurred at different magnetic fields. This positive MR disappears at high temperature as one moves away from the size-induced FM-M phase.

In the case of PCMO 20 as shown in figure 6(a), the maximum positive MR is observed at the forward magnetic field of 1.2 T and at 5.2 T in the reverse sweep for the measurements at 60 K. This R–H curve shows a non-closure of the hysteresis loop. The positive MR disappears at 80 K (with a closure of hysteresis) and at 120 K (with a non-closure of hysteresis). In the case of PCMO 40 as plotted in figure 6(b), the positive MR appears at 1 T in the forward sweep and at 5.2 T in the reverse direction, and is suppressed at 80 K and 120 K, giving way to negative MR with closure and non-closure hysteresis R–H loops, respectively. As shown in figure 6(c), in the case of PCMO NWs, the positive MR appears at 2 T in the forward magnetic field sweep and at 5.5 T in the reverse direction measured at 70 K. It disappears at high temperatures of 100, 120 and 140 K. Similar results (the presence of both positive and negative MR) were observed and were attributed to AFM ordering in the presence of FM interaction, even though the large positive MR is observed only after the sample is heated above 200 K before the data were taken at each temperature [37]. The aforementioned explanation might be applicable in the present case too, as these samples do have a certain fraction of anti-ferromagnetic phase, as shown from the magnetization

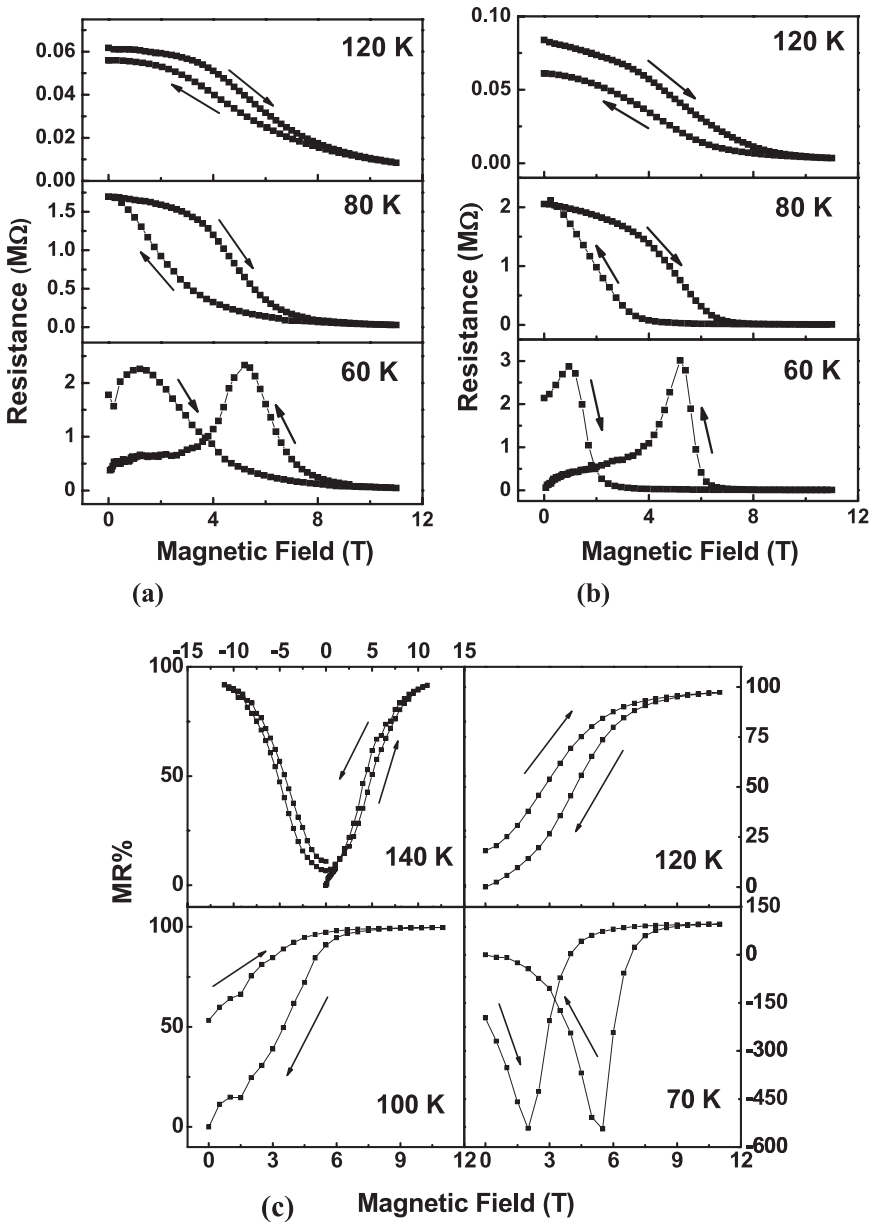

Figure 6. Isothermal variation of resistance R with magnetic field in forward and reverse directions as indicated by the pointed arrows for PCMO 20 (a) and PCMO 40 (b) measured at 60, 80 and 120 K. Plots of the isothermal MR (MR $= (\frac{\rho_0 - \rho_H}{\rho_0}) \times 100$) variation with the magnetic field sweep in forward and reverse directions as indicated by the pointed arrows measured at different temperatures 70, 100, 120 and 140 K ($0 \rightarrow 11$ T $\rightarrow 0 \rightarrow -11$ T $\rightarrow 0$) (70 K); ($0 \rightarrow 11$ T $\rightarrow 0$) (100, 120, 140 K) for PCMO NW (c).

measurements. Here, the data are taken just after cooling the samples to their respective lowest temperatures. Hence we argue that the observed positive MR is the intrinsic nature of the sample but not because of the temperature/field cycling effects. Surprisingly, it is seen from these figures that the resistance of the sample does not recover back to the original value on decreasing the magnetic fields to zero, showing large hysteresis (R–H) loops at the lowest temperatures of all the samples studied. These R–H curves show less hysteresis with the increase of temperature, i.e. these samples exhibit a strong magnetic memory effect. It is also found that the MR increases sharply at lower magnetic fields and saturates at relatively high fields beyond 7.5 T. Similar magnetic memory effects have been observed in nanoring networks of LCMO CMR nanomanganites [38]. Hence, here, it appears feasible to consider nanoscale CO manganites as potential materials for device applications.

5. Conclusions

The main experimental findings of the present investigation are summarized below.

Conventional magnetization measurements show the suppression of the CO phase and the size-induced ferromagnetic phase in PCMO nanoparticles. Magnetization measurements, carried out using a novel protocol, unveiled the presence

of existing magnetic phases, namely ferromagnetic and anti-ferromagnetic, which are tunable. The FM phase is the dominant equilibrium phase and is irreversible. It is attributable to size induced surface disorder thus bringing out the similarities between the size- and doping-induced disorders. The associated features give ample evidence for the occurrence of a first order phase transition (FOPT) which is arrested at low temperatures; and PCMO nanoparticles (PCMO 20 and PCMO 40) are shown to exhibit a 'magnetic glassy' state. The CO phase is shown to be softened with decreasing particle size.

Detailed transport data show the size-induced insulator–metal transition, and the obtained anomalous resistive hysteresis loops indicate the simultaneous presence of both metallic and insulating phases at the lowest temperatures studied; occurrence of colossal magneto-resistance (CMR) of 99.7% and strong magnetic memory effects are observed in resistive hysteresis (R–H) measurements, expected to be applicable in the fabrication of magnetic memory devices. Combined results obtained from novel magnetization and magneto-transport measurements—touching upon competing magnetic and electronic phases within nanoscale CO manganites—will likely stimulate general theoretical interest.

Acknowledgments

SSR acknowledges the CSIR, Government of India for financial support. The authors acknowledge the DST, Government of India for funding the 14 Tesla-PPMS-VSM used in these measurements located in IUC, Indore (UGC-DAE-CSR) and for providing the JANIS-made low temperature high magnetic field transport set-up located in the Indian Institute of Science, Bangalore, India. The authors benefited from fruitful discussions with Dr P Chaddah and Dr A Banerjee. SVB thanks DST India for NSTI project funding.

References

[1] Zimmermann M V, Hill J P, Gibbs D, Blume M, Casa D, Keimer B, Murakami Y, Tomioka Y and Tokura Y 1999 *Phys. Rev. Lett.* **83** 4872
[2] Okimoto Y, Tomioka Y, Onose Y, Otsuka Y and Tokura Y 1998 *Phys. Rev.* B **57** R9377
[3] Yang Z Q, Hendrikx R W A, Bentum P J M v and Aarts J 2002 *Europhys. Lett.* **58** 864
[4] Kajimoto R, Yoshizawa H, Tomioka Y and Tokura Y 2001 *Phys. Rev.* B **63** 212407
[5] Zhang Y Q, Zhu Y L and Zhang Z D 2007 *J. Appl. Phys.* **101** 063919
[6] Dutta A, Gayathri N and Ranganathan R 2003 *Phys. Rev.* B **68** 054432
[7] Dey P and Nath T K 2006 *Appl. Phys. Lett.* **89** 163102
[8] Bibes M, Balcells L I, Fontcuberta J, Wojcik M, Nadolski S and Jedryka E 2003 *Appl. Phys. Lett.* **82** 928
[9] Yu J Y, Tang S L, Zhang X K, Zhai L, Shi Y G, Deng Y and Du Y W 2009 *Appl. Phys. Lett.* **94** 182506
[10] Reyes Calvo M, Fernández-Rossier J, Palacios J J, Jacob D, Natelson D and Untiedt C 2009 *Nature* **458** 1150
[11] Han S, Li C, Liu Z, Lei B, Zhang D, Jin W, Liu X, Tang T and Zhou C 2004 *Nano Lett.* **4** 1241
[12] Dolz M I, Bast W, Antonio D, Pastoriza H, Curiale J, Sánchez R D and Leyva A G 2008 *J. Appl. Phys.* **103** 083909
[13] Rao S S, Anuradha K N, Sarangi S and Bhat S V 2005 *Appl. Phys. Lett.* **87** 182503
Anuradha K N, Rao S S and Bhat S V 2007 *J. Nanosci. Nanotechnol.* **5** 1775
[14] Rao S S, Tripathy S, Pandey D and Bhat S V 2006 *Phys. Rev.* B **74** 144416
[15] Rao S S and Bhat S V 2009 *J. Phys. D: Appl. Phys.* **42** 075004 and references therein
[16] Rao S S and Bhat S V 2007 *J. Nanosci. Nanotechnol.* **7** 2025
[17] Rao S S and Bhat S V 2009 *J. Phys.: Condens. Matter* **21** 196005 and references therein
[18] Dong S, Gao F, Wang Z Q, Liu J-M and Ren Z F 2007 *Appl. Phys. Lett.* **90** 082508
[19] Sarkar T, Mukhopadhyay P K, Raychaudhuri A K and Banerjee S 2007 *J. Appl. Phys.* **101** 124307
[20] Gao F, Li P L, Weng Y Y, Dong S, Wang L F, Lv L Y, Wang K F and Liu J-M 2007 *Appl. Phys. Lett.* **91** 072504
[21] Biswas A and Das I 2007 *Appl. Phys. Lett.* **91** 013107
[22] Banerjee A, Pramanik A K, Kumar K and Chaddah P 2006 *J. Phys.: Condens. Matter* **18** L605
[23] Banerjee A, Mukherjee A, Kumar A K and Chaddah P 2006 *Phys. Rev.* B **74** 224445
[24] Banerjee A, Kumar K and Chaddah P 2009 *J. Phys.: Condens. Matter* **21** 026002 and references therein
[25] Martin C, Maignan A, Hervieu M and Raveau B 1999 *Phys. Rev.* B **60** 12191
[26] Woodward P M, Vogt T, Cox D E, Arulraj A, Rao C N R, Karen P and Cheetham A K 1998 *Chem. Mater.* **10** 3652
[27] Li X, Zhang H, Chi F, Li S, Xu B and Zhao M 1993 *Mater. Sci. Eng.* B **18** 209
[28] Zysler R D, Ramos C A, De Biasi E, Romero H, Ortega A and Fiorani D 2000 *J. Magn. Magn. Mater.* **221** 37
[29] Tronc E, Ezzi A, Cherkaoui R, Chaneac C, Nogues M, Kachkachi H, Fiorani D, Testa A M, Greneche J M and Jolivet J P 2000 *J. Magn. Magn. Mater.* **221** 63
[30] Manekar M A, Chaudhary S, Chattopadhyay M K, Singh K J, Roy S B and Chaddah P 2001 *Phys. Rev.* B **64** 104416
[31] Zhang Y Q, Zhang Z D and Aarts J 2005 *Phys. Rev.* B **70** 132407
[32] Curiale J, Sanchez R D, Troiani H E, Ramos C, Pastoriza H, Leyva A G and Levy P 2007 *Phys. Rev.* B **75** 224410
[33] Balcells L, Fontcuberta J, Martínez B and Obradors X 1998 *Phys. Rev.* B **58** R14697
[34] Kar S, Sarkar J and Raychaudhuri A K 2006 *IEEE Trans. Nanotechnol.* **5** 707
[35] Kumar D, Sankar J, Narayan J, Singh R K and Majumdar A K 2002 *Phys. Rev.* B **65** 094407
[36] Venkataiah G, Krishna D C, Vithal M, Rao S S, Bhat S V, Prasad V, Subramanyam S V and Venugopal Reddy P 2005 *Physica* B **357** 370
[37] Mahendiran R, Mahesh R, Gundakaram R, Raychaudhuri A K and Rao C N R 1996 *J. Phys.: Condens. Matter* **8** L455
[38] Zhu M H, Zhao Y G, Cai W, Wu X S, Gao S N, Wang K, Luo L B, Huang H S and Lu L 2007 *Phys. Rev.* B **75** 134424